Mathematical modeling of the hydrogen evolution process on nickel, cobalt, and Co-Ni alloy coatings in acidic and alkaline environments

Aleksandra J. Domańska[a], Piotr M. Skitał[b]

[a]Doctoral School of the Rzeszów University of Technology, 35-959 Rzeszów, Poland, a.domanska@stud.prz.edu.pl, ORCID: 0000-0001-9663-2827

[b]Faculty of Chemistry, Rzeszów University of Technology, 35-959 Rzeszów, Poland, pskital@prz.edu.pl, ORCID: 0000-0002-8664-7563

Corresponding author: Piotr M. Skitał, pskital@prz.edu.pl

Abstract. The content of this study discusses the kinetic issues of hydrogen evolution on metallic surfaces. For this purpose, the electrochemical deposition of Ni, Co, and Co-Ni alloy coatings from chloride baths on chromium-nickel steel (304) substrates was conducted. The deposited materials were then used as the cathode for electrolytic hydrogen evolution. Due to differences in electrochemical reaction mechanisms, the studies were carried out in acidic (0.5 M H_2SO_4) and alkaline (1 M NaOH) environments. Using different polarization rates (0.05; 0.1; 0.2; 0.5; 1; 2 V/s), cyclic voltammetry (CV) curves were recorded, showing the current intensity as a function of potential. Based on the experimental H_2 evolution curves and the ESTYM_PDE program, a mathematical model was developed to determine the parameters of the hydrogen evolution reaction (HER) on the metal and alloy coatings.

Keywords: hydrogen evolution reaction, water splitting, electrolysis, alloy Co–Ni

1. INTRODUCTION

The hydrogen evolution reaction (HER) is currently one of the most thoroughly studied electrochemical reactions due to the great interest in hydrogen as an energy carrier. Green hydrogen, obtained by electrolysis, can meet the growing demand for energy. (Khan, 2023, Chmielniak, 2021). The planned development of the hydrogen economy includes green and potentially blue hydrogen. The former is a gas produced in an environmentally friendly manner, i.e., through electrolysis powered by renewable energy sources (RES) (Yu et al., 2024). The latter, blue hydrogen, is a variant of grey hydrogen, which is produced from fossil fuels. However, in the case of blue hydrogen, carbon capture, utilization, and storage (CCUS) is employed to manage the by-product carbon dioxide (IRENA, 2019). Currently, over 95% of hydrogen is produced from fossil fuels (Komorowska et al., 2023), including steam methane reforming, petroleum reforming, and coal gasification (Shiva and Lim, 2022, Riera et al., 2023). Cost-effective production of green hydrogen is a crucial element of a sustainable hydrogen economy (Lohmann-Richters et al., 2021, Hota et al., 2023).

Water electrolysis involves the electrochemical splitting of water molecules through the application of an external electric current (Daoudi and Bounahmidi, 2023). The decomposition of water can occur in acidic, neutral, and alkaline environments. The reaction proceeds most favorably with strong electrolytes (H_2SO_4, KOH, NaOH) due to their high conductivity (Bespalko and Mizeraczyk, 2022). The electrochemical system comprises two electrodes: the hydrogen evolution reaction (HER) occurs at the cathode surface, while the oxygen evolution reaction (OER) takes place at the anode. The electrolyzer equipped with noble metal electrocatalyst such as Pt, Pd, Ir, and Ru enhances the efficiency of hydrogen evolution reaction (Raveendran et al., 2023). However, the high costs and material shortages hinder the large-scale development of energy devices (Li et al., 2023). Transition metals such as nickel and cobalt exhibit electrocatalytic properties for both hydrogen (Chun and Chun, 2024) and oxygen (Krivina et al., 2022) evolution reactions. Nickel alloys can absorb amounts of hydrogen into their structure and subsequently desorb it, which is useful not only for the evolution process but also for hydrogen storage (Baraniak et al., 2024). Enhancing ion adsorption is particularly important in alkaline environments where hydrogen ion concentration is low (Goyal and Koper, 2021). Current literature indicates that modifying the composition or structure of materials based on these metals gives satisfactory results. Li et al. (2022) conducted a finite element method simulation, finding that the electric field of nickel nanoparticles increases ion adsorption, facilitating kinetics and mass transfer on the electrodes. Previous work (Skitał and Domańska, 2022) involving the investigation, parameter determination, and mathematical

modeling of the hydrogen evolution process with simultaneous cobalt deposition confirmed the catalytic effect of Co on HER. Gupta et al. (2023), in their review paper, attribute the exceptional catalytic activity of cobalt due to its partially filled d orbital. In addition, structural defects, such as vacancies located in the cobalt crystal lattice, make these sites even more catalytically active. Dymerska et al. (2020) demonstrated that Ni and Co particles as additives enhance the efficiency of the electrocatalyst by providing a large number of active sites.

This study involves the electrochemical deposition of nickel (Ni), cobalt (Co), and their alloy (Co-Ni) coatings to enhance the efficiency of the hydrogen evolution reaction (HER) on chromium-nickel materials. Due to the presence of different electrolysis mechanisms, the electrocatalytic properties for hydrogen evolution in both acidic and alkaline environments are presented. The establishment of a mathematical model for the hydrogen evolution process on electrodeposited coatings allows for the verification of surfaces in terms of process electrocatalysis. Furthermore, it enables the utilization of existing knowledge and relationships to design new and improved solutions that increase and develop the hydrogen economy.

2. EXPERIMENTAL PART AND NUMERICAL PROCEDURES

2.1. Electrodeposition of coatings

The surface of the chromium-nickel substrate (304) was electropolished for 15 minutes using a current density j of 21 A/dm². The solution used consisted of: 0.3 dm³ of 85% H_3PO_4, analytical grade (CHEMPUR), 0.185 dm³ of concentrated H_2SO_4, analytical grade (CHEMPUR) and 0.015 dm³ of distilled water.

The coatings were deposited using three chloride baths, the compositions and current parameters of which are presented in Table 1. The compounds used were sourced from CHEMPUR and demonstrated analytical purity levels. The deposited chromium-nickel ($d = 4$ mm), platinum electrode, and saturated silver chloride electrode (Ag/AgCl) served as the working electrode, counter electrode, and reference electrode, respectively. The samples were deposited in a thermostated electrolyzer (25°C) using the chronopotentiometric (CP) technique with EPSILON (BASi) equipment.

Table 1. Current parameters of electrodeposition, electrolyte composition, and theoretical coating thicknesses.

Coating designation	Electrolyte composition	Current density j, mA/cm^2	theoretical thicknesses s, μm
Ni	0.06 M NiCl$_2$ 0.5 M H$_3$BO$_3$	10	1 and 5
Co	0.06 M CoCl$_2$ 0.5 M H$_3$BO$_3$	3	
Co-Ni	0.06 M NiCl$_2$ 0.04 M CoCl$_2$ 0.5 M H$_3$BO$_3$	3 and 10	1
		10	5

Based on the theoretical coating thicknesses of 1 and 5 μm, the value of the electric charge required to flow through the system to deposit the amount of material corresponding to the assumed thickness was calculated.
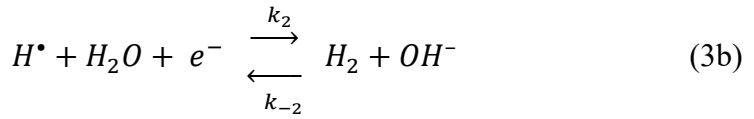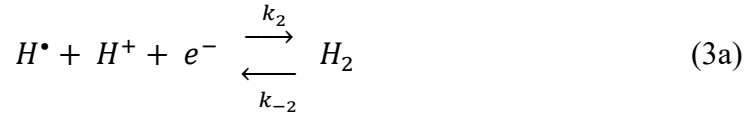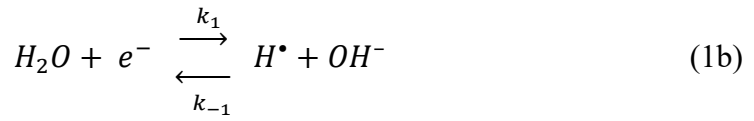
2.2. Hydrogen evolution

The electrodeposited coatings served as the cathode during the electrolytic hydrogen evolution. The process was conducted in two environments: acidic (using 0.5 M H$_2$SO$_4$) and alkaline (using 1 M NaOH). The EPSILON (BASi) equipment and the same thermostated setup (25°C) with an identical electrode arrangement were used again. The potential values were then converted relative to the standard hydrogen electrode (SHE). Cyclic voltammetry (CV) curves were recorded for each surface. Six scanning series were conducted for each sample, using different scan rates v in the following order: 0.05; 0.1; 0.2; 0.5; 1; and 2 V/s. Before starting the measurements, the electrolyte was deaerated with argon for 15 minutes, and for 3 minutes between series. Before each subsequent scan, i.e., before changing the scan rate, the system was deaerated for 20 seconds. Depending on the reaction environment, different reversal potentials were used for the studies. In sulfuric acid, gaseous hydrogen desorption occurred faster at lower scan rates, disrupting the measurement; hence, individual reversal potentials were set for each surface. In NaOH, a constant value of -1.501 V was used for all coatings and scan rates.

2.3. Mathematical modeling

Electrochemical calculations were conducted using the ESTYM_PDE software. This program solves and estimates parameters of one-dimensional mass and heat transfer coupled with chemical and electrochemical reactions based on partial differential equations (PDE). Bard et al. (2022) have thoroughly described the diffusion PDE based on Fick's second law, along with

boundary conditions defining the concentration dependence over time. The presented model accounts for HER without oxidation reactions.

The mathematical model of the process accounts for the catalytic effect of hydrogen evolution by relating (conditioning) the hydrogen evolution rate as a function of the type and thickness of the layer deposited on the electrode. The model describes the following set of electrochemical and chemical reactions:

$$H^+ + e^- \underset{k_{-1}}{\overset{k_1}{\rightleftharpoons}} H^\bullet \tag{1a}$$

$$H_2O + e^- \underset{k_{-1}}{\overset{k_1}{\rightleftharpoons}} H^\bullet + OH^- \tag{1b}$$

$$2H^\bullet \overset{k_{H^\bullet}}{\rightarrow} H_2 \tag{2}$$

$$H^\bullet + H^+ + e^- \underset{k_{-2}}{\overset{k_2}{\rightleftharpoons}} H_2 \tag{3a}$$

$$H^\bullet + H_2O + e^- \underset{k_{-2}}{\overset{k_2}{\rightleftharpoons}} H_2 + OH^- \tag{3b}$$

The mass balance of the individual chemical compounds is described by a set of equations (4) - (6) for a planar electrode:

$$\frac{\partial c_{H^+}}{\partial t} = D_{H^+} \frac{\partial^2 c_{H^+}}{\partial x^2} \tag{4a}$$

$$\frac{\partial c_{H_2O}}{\partial t} = D_{H_2O} \frac{\partial^2 c_{H_2O}}{\partial x^2} \tag{4b}$$

$$\frac{\partial c_{H^\bullet}}{\partial t} = D_{H^\bullet} \frac{\partial^2 c_{H^\bullet}}{\partial x^2} - k_{H^\bullet} c_{H^\bullet}^2 \tag{5}$$

$$\frac{\partial c_{H_2}}{\partial t} = D_{H_2} \frac{\partial^2 c_{H_2}}{\partial x^2} + k_{H^\bullet} c_{H^\bullet}^2 \tag{6}$$

along with the relevant conditions.

1. Initial conditions

for $t = 0$ and $x \geq 0$: $c_{H^+} = c_{H^+}^0$, $\quad c_{H^\bullet} = c_{H_2} = 0$ \hfill (7a)

for $t = 0$ and $x \geq 0$: $c_{H_2O} = c_{H_2O}^0$, $\quad c_{H^\bullet} = c_{H_2} = 0$ \hfill (7a)

2. Boundary conditions

2.1. for $t > 0$ and $x = 0$:

$$D_{H^+} \frac{\partial c_{H^+}}{\partial x} = +k_1 c_{H^+} exp\left(-\frac{\alpha_1 F(E-E_0)}{RT}\right) - k_{-1} c_{H^\bullet} exp\left(\frac{(1-\alpha_1)F(E-E_0)}{RT}\right) \tag{8a}$$

$$D_{H_2O} \frac{\partial c_{H_2O}}{\partial x} = +k_1 c_{H_2O}\, exp\left(-\frac{\alpha_1 F(E-E_0)}{RT}\right) - k_{-1} c_{H\cdot}\, exp\left(\frac{(1-\alpha_1)F(E-E_0)}{RT}\right) \tag{8b}$$

$$D_{H\cdot} \frac{\partial c_{H\cdot}}{\partial x} = -k_1 c_{H^+}\, exp\left(-\frac{\alpha_1 F(E-E_0)}{RT}\right) + k_{-1} c_{H\cdot}\, exp\left(\frac{(1-\alpha_1)F(E-E_0)}{RT}\right) +$$

$$k_2 c_{H\cdot}\, exp\left(-\frac{\alpha_2 F(E-E_0)}{RT}\right) - k_{-2} c_{H_2}\, exp\left(\frac{(1-\alpha_2)F(E-E_0)}{RT}\right) \tag{9}$$

$$D_{H_2} \frac{\partial c_{H_2}}{\partial x} = -k_2 c_{H\cdot}\, exp\left(-\frac{\alpha_2 F(E-E_0)}{RT}\right) + k_{-2} c_{H_2}\, exp\left(\frac{(1-\alpha_2)F(E-E_0)}{RT}\right) \tag{10}$$

where, c_{H^+} are the ion concentrations in solution (mol/cm^3), $c_{H\cdot}$ is the hydrogen radical concentration. The symbol E_0 means the standard potential of the redox system ($E^0_{H^+}$ = 0.000 V and E^0_{H2O} = -0.828 V), α the transfer coefficient of the cathodic process and x indicates the distance from the electrode surface. The $k_{H\cdot}$ constant was estimated that its value must be greater than 10^5 s^{-1}, resulting in no oxidation peak on the theoretical curve (according to the experiment).

2.2. for $t > 0$ and $x \rightarrow \infty$:

$$c_{H^+} = c^0_{H^+}, c_{H\cdot} = c_{H_2} = 0 \tag{11a}$$

$$c_{H_2O} = c^0_{H_2O}, c_{H\cdot} = c_{H_2} = 0 \tag{11b}$$

The diffusion layer thickness δ considered in the model defines the relation diffusion coefficient D and experimental time t in the form of dependencies $\delta = 6\sqrt{D \cdot t}$.

By solving the system of equations (1) - (6) along with the the relevant initial and boundary conditions (7) - (11), the concentration-time dependence of all chemical compounds on the electrode and in the solution can be found.

The current can be described by the equations:

$$I_1 = FAD_{H^+} \frac{\partial c_{H^+}}{\partial x} \tag{12a}$$

$$I_1 = FAD_{H_2O} \frac{\partial c_{H_2O}}{\partial x} \tag{12b}$$

$$I_2 = FAD_{H^+} \frac{\partial c_{H^+}}{\partial x} + FAD_{H\cdot} \frac{\partial c_{H\cdot}}{\partial x} \tag{13a}$$

$$I_2 = FAD_{H_2O} \frac{\partial c_{H_2O}}{\partial x} + FAD_{H\cdot} \frac{\partial c_{H\cdot}}{\partial x} \tag{13b}$$

$$I_{Total} = I_1 + I_2 \tag{14}$$

Simulations were performed until the degree of fit was the best possible, as indicated by the constant value of the ASD$_\%$ parameter.

$$ASD_\% = \frac{\sqrt{\Sigma(y-\hat{y})^2}}{\sqrt{\Sigma(y)^2}} \cdot 100\% \tag{15}$$

where: y – experimental current intensity, ŷ – calculated current intensity.

3. RESULTS AND ANALYSIS

3.1. Hydrogen evolution reaction curves

The recorded HER curves are summarized in Fig. 1 including measurements for all surfaces at scan rate 0.2 V/s. Graphs A and B represent an acidic and alkaline environment, respectively. Depending on the electrolyte used, it is possible to indicate the structure that exhibits the smallest overpotential and the maximum current obtained. In an alkaline environment, the best parameters are achieved by an alloy coating (Co-Ni) with a thickness of 5 μm, while in an acidic environment, a cobalt coating of the same thickness shows the best parameters. The highest efficiency obtained for cobalt coating in acidic medium can be explained by the fact that cobalt, with three unfilled d orbitals (compared to two for Ni), forms bonds that are neither too strong nor too weak. This ensures optimal absorption of chemical individuals reaching the catalyst surface and desorption of the product (Gupta et al., 2023). Hydrogen release in an alkaline medium is preceded by a slow dissociation of water, so the process is slower than in an acidic electrolyte (Ďurovič et al., 2021). Lyu et al. (2024) indicate in their work the synergistic effect of Ni and Co in alkaline medium. Lupi et al. (2009), on the other hand, explains that the synergistic effect of this alloy is that Ni provides a low hydrogen superconducting potential and cobalt provides high hydrogen adsorption. This allows for a higher value of exchange current density.

The reference point was the uncoated 304 electrode surface (black line), and the increase in the value of the current density is 2.75 times and the shift of the potential value in the positive direction is 169 mV for the acidic environment. In an alkaline environment, the values are 2.07 times and 206 mV.

In an acidic environment, the thickness of the nickel coating did not affect the overpotential or the maximum current. In the case of the cobalt coating, increasing the thickness of the deposited Co layer allowed for obtaining a smaller overpotential, while the maximum current values were practically equal. In the alkaline electrolyte, it was noticed that the electrode material affects the overpotential of hydrogen evolution, while increasing the coating thickness allows for achieving higher values of maximum currents.
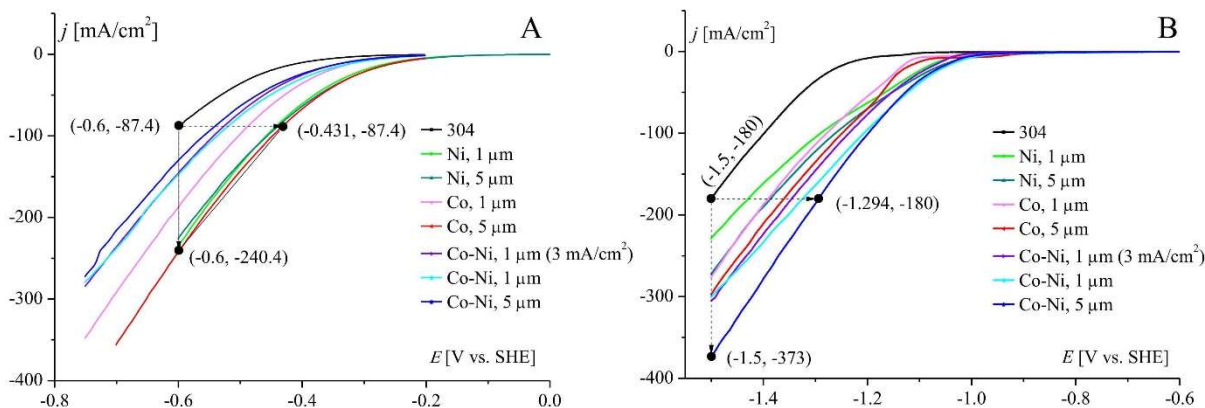
Fig. 1. HER curves of all surfaces at scan rate 0.2 V/s. Graph A represents an acidic environment, while B represents an alkaline environment.

3.2. Kinetic parameters of hydrogen evolution

Mathematical modelling of hydrogen reduction involved the estimation and determination of kinetic parameters such as the reaction rate constant k and the transfer coefficient α. The reaction rate constant indicates the efficiency of the electrochemical reaction. Surfaces that exhibited the highest value of the rate constant are characterized by the best catalytic properties in the given environment. Table 2 presents the estimated values of the parameters. The lowest value of the rate constant was determined for the electropolished chromium-nickel (304) surface. Hydrogen evolution in an acidic environment occurs more efficiently than in an alkaline environment due to the higher concentration of H^+. Higher values of the reaction rate constant in an H_2SO_4 environment confirm the validity of the mathematical model considering Volmer and Tafel reactions, because the absolute values of the rate constants are higher than in alkaline medium. Moreover, in acidic environment the highest value of the constant $k = 5.0 \times 10^{-5}$ cm/s recorded for a 5 µm thick cobalt coating is 9.26 - times higher compared to uncoated electrode ($k = 5.4 \times 10^{-6}$ cm/s). This confirms the validity of co-depositing cobalt as a component of coatings used in the hydrogen evolution process. In an alkaline electrolyte, based on experimental results and conducted estimations, the best catalytic properties are exhibited by alloy coatings deposited using a current density of 10 mA/cm^2 ($k = 3.3 \times 10^{-6}$ cm/s), where a 15 - times increase in the rate constant was observed ($k = 2.2 \times 10^{-7}$ cm/s).

By analysing the parameter α in a given environment, it can be observed that the values for the coatings differ slightly from each other. The difference is greater when comparing the parameter between the coatings and the chromium-nickel steel surface. However, when comparing with

the reaction rate constants, it can be concluded that coatings characterized by higher k values show lower α values at the same time.

Table 2. Model parameters of the hydrogen evolution process in an acidic and alkaline environment on the chromium-nickel surface and coatings along with the standard deviation, determined considering the Volmer and Tafel reactions.

Material of the working electrode	Parameters in an acidic environment $\pm SD$		Parameters in an alkaline environment $\pm SD$	
	k_1, cm/s	α_1	k_1, cm/s	α_1
304	$(5.4 \pm 0.6) \cdot 10^{-6}$	0.221 ± 0.004	$(2.2 \pm 1.2) \cdot 10^{-7}$	0.203 ± 0.019
Ni, 1 μm, 10 mA/cm^2	$(2.6 \pm 0.9) \cdot 10^{-5}$	0.205 ± 0.017	$(1.7 \pm 0.2) \cdot 10^{-6}$	0.129 ± 0.004
Ni, 5 μm, 10 mA/cm^2	$(3.1 \pm 0.9) \cdot 10^{-5}$	0.193 ± 0.014	$(1.9 \pm 0.3) \cdot 10^{-6}$	0.131 ± 0.005
Co 1 μm, 3 mA/cm^2	$(2.7 \pm 0.5) \cdot 10^{-5}$	0.184 ± 0.008	$(1.1 \pm 0.1) \cdot 10^{-6}$	0.152 ± 0.005
Co 5 μm, 3 mA/cm^2	$(5.0 \pm 1.2) \cdot 10^{-5}$	0.174 ± 0.011	$(1.6 \pm 0.2) \cdot 10^{-6}$	0.142 ± 0.007
Co-Ni, 1 μm, 3 mA/cm^2	$(2.1 \pm 0.4) \cdot 10^{-5}$	0.183 ± 0.007	$(2.2 \pm 0.6) \cdot 10^{-6}$	0.133 ± 0.007
Co-Ni, 1 μm, 10 mA/cm^2	$(2.7 \pm 0.3) \cdot 10^{-5}$	0.173 ± 0.005	$(3.2 \pm 0.8) \cdot 10^{-6}$	0.118 ± 0.008
Co-Ni, 5 μm, 10 mA/cm^2	$(1.9 \pm 0.3) \cdot 10^{-5}$	0.182 ± 0.006	$(3.3 \pm 1.1) \cdot 10^{-6}$	0.125 ± 0.010

During the estimation phase, it was observed that curve fitting in a NaOH environment is much worse than in acid. Therefore, in the process of modeling hydrogen evolution in an alkaline environment, the Heyrovsky reaction was additionally taken into account. The parameters along with their values are presented in Table 3, where the subscript 1 represents the Volmer reaction parameters, and 2 represents the Heyrovsky reaction parameters.

Table 3. Parameters of the hydrogen evolution process in an alkaline environment on the chromium-nickel surface and coatings along with the standard deviation, determined considering the Volmer, Tafel, and Heyrovsky reactions.

Material of the working electrode	Parameters in an alkaline environment $\pm SD$			
	k_1, cm/s	k_2, cm/s	α_1	α_2
304	$(2.1 \pm 0.3) \cdot 10^{-7}$	$(7.5 \pm 3.2) \cdot 10^{-8}$	0.170 ± 0.005	0.661 ± 0.086
Ni, 1 μm, 10 mA/cm^2	$(1.2 \pm 0.2) \cdot 10^{-6}$	$(1.5 \pm 1.0) \cdot 10^{-5}$	0.115 ± 0.005	0.551 ± 0.029
Ni, 5 μm, 10 mA/cm^2	$(1.1 \pm 0.1) \cdot 10^{-6}$	$(1.6 \pm 1.0) \cdot 10^{-5}$	0.126 ± 0.006	0.734 ± 0.014
Co 1 μm, 3 mA/cm^2	$(8.5 \pm 0.9) \cdot 10^{-7}$	$(7.5 \pm 7.0) \cdot 10^{-7}$	0.132 ± 0.003	0.671 ± 0.112

Co 5 μm, 3 mA/cm^2	$(1.2 \pm 0.2) \cdot 10^{-6}$	$(6.3 \pm 6.1) \cdot 10^{-7}$	0.122 ± 0.005	0.673 ± 0.089
Co-Ni, 1 μm, 3 mA/cm^2	$(1.5 \pm 0.4) \cdot 10^{-6}$	$(4.0 \pm 2.2) \cdot 10^{-6}$	0.116 ± 0.007	0.580 ± 0.043
Co-Ni, 1 μm, 10 mA/cm^2	$(1.8 \pm 0.2) \cdot 10^{-6}$	$(2.0 \pm 3.0) \cdot 10^{-6}$	0.111 ± 0.004	0.783 ± 0.034
Co-Ni, 5 μm, 10 mA/cm^2	$(1.9 \pm 0.3) \cdot 10^{-6}$	$(2.9 \pm 4.0) \cdot 10^{-5}$	0.182 ± 0.006	0.182 ± 0.030

The visual fitting of the described model to the experimental data in both hydrogen evolution environments can be observed in Fig. 2. In these cases, the modelling only considers the Volmer and Tafel reactions (VT model). It can be noted that the fitting of the model curves to the experimental ones for the base is significantly worse compared to the acid. Analysing the curves and comparing them with the set that only considers the Tafel reaction indicates a significantly better fit of the curves by including the Heyrovsky reaction (VTH model).

In Fig. 2 we can visually observe the degree of fit of the models to the experimental data, but a more precise comparison (mathematical) requires the use of an appropriate parameter. The ASD$_\%$ parameter defines the degree of mismatch in percentage terms, so the smaller its value, the better the fit of the model data to the experimental data. The information on the fit of the model data to the experimental data presented in Fig. 3 corresponds to the visual fit shown in Fig. 2. Including the Heyrovsky reaction in the case of hydrogen evolution in NaOH increases the fit, and consequently, the model better describes the electrochemical process. Moreover, this reaction is necessary to obtain a fit similar to that of hydrogen evolution in acid, which is described only by two reactions (Volmer and Tafel). This is consistent with the statement that the mechanism of hydrogen evolution in acid is less complicated. The acidic environment provides the presence of H$^+$ ions, which are adsorbed on the electrode surface. In the alkaline environment, the initial stage is the slow dissociation of water, which reduces the rate of HER (Wang et al., 2021).
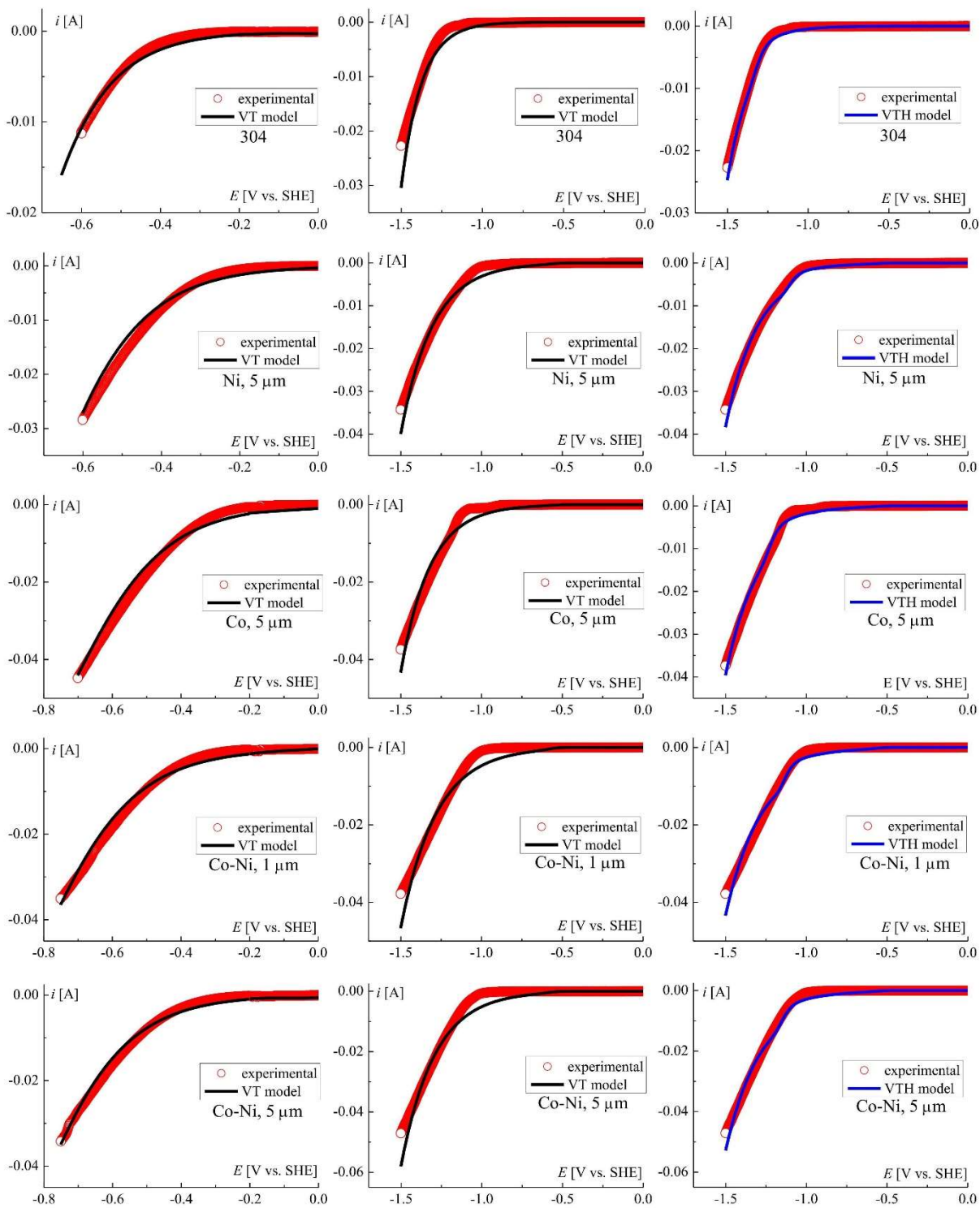
Fig. 2. Qualitative fit of the VT (black lines) and VTH (blue lines) models to the experimental data (red dots) recorded at a scan rate of 0.2 V/s in acidic (column 1) and alkaline environments (column 2, 3).
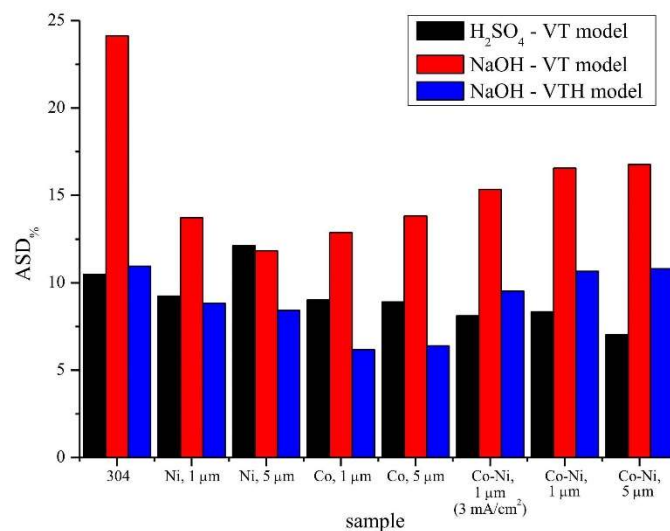
Fig. 3. Quantitative degree of fit of the model to the experimental data; the lower the value of the ASD% parameter, the better the fit.

The determined parameter values of the approximated percentage standard deviation (ASD%) obtained by mathematical modeling of the hydrogen evolution process are between 6.2% - 24.1%. The best fit in NaOH solution was achieved for a 1 μm cobalt-coated electrode, and the weakest fit without coating. On the other hand, in H_2SO_4 solution, the best match between calculated and experimental results was obtained for 5 μm Co-Ni coating, and the weakest for 5 μm Ni coating. As can easily be seen, they depend heavily on the type of coating, so a more clear picture is obtained when we count the corresponding average values along with the standard deviation. They are respectively: 9.2 ± 1.6, 15.6 ± 3.8 and 9.0 ± 1.9 for the VT model in H_2SO_4, the VT model in NaOH and the VTH model in NaOH.

4. CONCLUSIONS

1. The presence of a coating of Ni, Co and Co-Ni alloy on the chromonickel electrodes has a significant effect on the hydrogen evolution process, where the process occurs with greater efficiency.

2. The thickness of the deposited coating affects the hydrogen evolution process. Coatings with a thickness of 5 μm showed the best performance during the hydrogen evolution process in both acidic and alkaline environments.

3. The rate constants *k*, determined by mathematical modeling, show higher values on electrodes with deposited coatings compared to electrodes without coatings. In an acidic environment, there is no clear difference (trend) between coatings, except for the thickest cobalt coating, which shows the greatest catalytic effect. In an alkaline environment, the rate of

hydrogen evolution on Co-Ni alloy coatings is higher with respect to coatings made of single metals.

4. The model presented in this paper using only the Volmer-Tafel reaction allows for a very good fit in an acidic environment. In order to obtain a similar level of fit in NaOH environment, the Heyrovsky reaction had to be included in the model.

SYMBOLS

j - current density, A/dm^2, mA/cm^2

d - diameter of the working electrode, mm

s - theoretical thickness of the coating, μm

v - scan rate, V/s

k - reaction rate constant, cm/s

D - diffusion coefficient, cm^2/s

c - concentration, mol/dm^3, mol/cm^3

$k_{H\bullet}$ - recombination constant, cm^3/mol s

t - time, s

x - distance from the electrode, cm

F - Faraday's constant

E - potential, V

E_0 - zero potential, V

R - gas constant,

T - temperature, K

I, i - current, A, mA

A - electrode area, cm^2

y - experimental current intensity, A

$\hat{y}$ - calculated current intensity, A

SD - standard deviation

Greek symbols

α - transition factor

δ - diffusion layer thickness, cm

REFERENCES

1. Baraniak M., Staszak K., Kruszelnicka I., Ginter-Kramarczyk D., Góra W., Lota G., Regel-Rosocka M., 2024. From nickel waste solution to hydrogen storage alloys – An excellent example of circular economy implementation. *Sep. Purif. Technol.*, 328, 125063. DOI: 10.1016/j.seppur.2023.125063.

2. Bard A. J., Faulkner L. R., White H. S., 2022. *Elektrochemical Methods. Fundamental and Applications*. 3rd edition, Wiley, New York, xx-xx.

3. Bespalko S., Mizeraczyk J., 2022. Overview of the Hydrogen Production by Plasma-Driven Solution Electrolysis. *Energies*, 15, 7508. DOI: 10.3390/en15207508.

4. Chmielniak T., 2021. Harnessing Hydrogen. *Academia PAS*, 1, 72-78. DOI: 10.24425/academiaPAS.138416.

5. Chun J., Chun J. H., 2024. Hydrogen and deuterium adsorptions and their equilibrium isotope effect on tungsten in alkaline solutions. *Int. J. Hydrogen Energy*, 57, 121-125. DOI: 10.1016/j.ijhydene.2024.01.016.

6. Daoudi C., Bounahmidi T., 2023. Overview of alkaline water electrolysis modeling. *Int. J. Hydrogen Energy*, 49, 646-667. DOI: 10.1016/j.ijhydene.2023.08.345.

7. Dymerska A., Kukułka W., Wenelska K., Mijowska E., 2020. Two–Dimensional Molybdenum Diselenide Tuned by Bimetal Co/Ni Nanoparticles for Oxygen Evolution Reaction. *ACS Omega*, 2, 28730-28737. DOI: 10.1021/acsomega.0c04024.

8. Ďurovič M., Hnát J., Bouzek K., 2021. Electrocatalysts for the hydrogen evolution reaction in alkaline and neutral media. A comparative review. *J. Power Sources*, 493, 229708. DOI: 10.1016/j.jpowsour.2021.229708.

9. Goyal A., Koper M. T. M., 2021. The Interrelated Effect of Cations and Electrolyte pH on the Hydrogen Evolution Reaction on Gold Electrodes in Alkaline Media. *Angew. Chem. Int. Ed.*, 60, 13452–13462. DOI: 10.1002/anie.202102803.

10. Gupta S., Fernandes R., Patel R., Spreitzer M., Patel N., 2023. A review of cobalt-based catalysts for sustainable energy and environmental applications. *Appl. Catal., A*, 661, 119254. DOI: 10.1016/j.apcata.2023.119254

11. Hota P., Das A. Maiti D. K., 2023. A short review on generation of green fuel hydrogen through water splitting. *Int. J. Hydrogen Energy*, 48, 523-541. DOI: 10.1016/j.ijhydene.2022.09.264.

12. IRENA, 2019, Hydrogen: A renewable energy perspective., International Renewable Energy Agency, *2nd Hydrogen Energy Ministerial Meeting*, Tokyo, Japan.

13. Khan N. A., Rahman G., Nguyen T. M., Shah A. U. H. A., Pham C.Q., Tran M. X., Nguyen D. L. T., 2023. Recent Development of Nanostructured Nickel Metal‑Based Electrocatalysts for Hydrogen Evolution Reaction: A Review. *Top. Catal*., 66, 149–181. DOI: 10.1007/s11244-022-01706-2.

14. Komorowska A., Mokrzycki E., Gawlik L., 2023. Hydrogen production in Poland – the current state and directions of development. *Energy Policy Journal*, 26, 81-98. DOI: 10.33223/epj/170913.

15. Krivina R. A., Lindquist G. A., Beaudoin S. R., Stovalla T. N., Thompson W. L., Twighta L. P., Marsha D., Grzyb J., Fabrrizio K., Hutchisona J. E., Boettcher S. W., 2022. Anode Catalysts in Anion-Exchange-Membrane Electrolysis without Supporting Electrolyte: Conductivity, Dynamics, and Ionomer Degradation, *Adv. Mater.*, 34, 2203033. DOI: 10.1002/adma.202203033.

16. Li H. Cai C., Wang Q., Chen S., Fu J., Liu B., Hu Q., Hu K., Li H.m Hu J., Liu Q., Chen S., Liu M., 2022. High-performance alkaline water splitting by Ni nanoparticle-decorated Mo-Ni microrods: Enhanced ion adsorption by the local electric field. *Chem. Eng. J.*, 435, 134860. DOI: 10.1016/j.cej.2022.134860.

17. Li M., Wang X., Liu K., Zhu Z., Guo H., Li M., Du Han., Sun D., Li H., Huang K., Tang Y., Fu G., 2023. Ce-Induced Differentiated Regulation of Co Sites via Gradient Orbital Coupling for Bifunctional Water-Splitting Reactions. *Adv. Energy Mater.*, 13, 2301162. DOI: 10.1002/aenm.202301162.

18. Lupi C., Dell'Era A., Pasquali M., 2009. Nickel–cobalt electrodeposited alloys for hydrogen evolution in alkaline media. *Int. J. Hydrogen Energy*, 34, 2101-2106. DOI: 10.1016/j.ijhydene.2009.01.015.

19. Lyu LM. Li HJ. Tsai RS., Chen CF., Chang YC., Chuang YC., Li CS., Chen JL., Chiu TW., Kuo CH., 2024. In Operando X‑ray Spectroscopic and DFT Studies Revealing Improved H_2 Evolution by the Synergistic Ni−Co Electron Effect in the Alkaline Condition. R*ACS Appl. Mater. Interfaces*, 16, 27329−27338. DOI: 10.1021/acsami.4c02613.

20. Lohmann-Richters F.P., Renz S., Lehnert W., Müller M., Carmo M., 2021. Review–Challenges and Opportunities for Increased Current Density in Alkaline Electrolysis by

Increasing the Operating Temperature. *J. Electrochem. Soc.*, 168, 114501. DOI: [10.1149/1945-7111/ac34cc](10.1149/1945-7111/ac34cc).

21. Raveendran A., Chandran M., Dhanusuraman R., 2023. A comprehensive review on the electrochemical parameters and recent material development of electrochemical water splitting electrocatalysts. *RSC Adv.*, 13, 3842-3876. DOI: [10.1039/d2ra07642j](10.1039/d2ra07642j).

22. Riera J. A., Lima R. M., Knio O. M., 2023. A review of hydrogen production and supply chain modeling and optimization, *Int. J. Hydrogen Energy*, 48, 13731-13755. DOI: 10.1016/j.ijhydene.2022.12.242.

23. Shiva K. S., Lim H., 2022. An overview of water electrolysis technologies for green hydrogen production. *Energy Rep.*, 8, 13793-13813. .DOI: 10.1016/j.egyr.2022.10.127.

24. Skitał P. M., Domańska A. J., 2022. Modeling of the Simultaneous Hydrogen Evolution and Cobalt Electrodeposition. *ChemPhysChem*, 23, e202200148. DOI: 10.1002/cphc.202200148.

25. Wang S., Lu A., Zhong CJ., 2021. Hydrogen production from water electrolysis: role of catalysts. *Nano Convergence*, 8, 4. DOI: [10.1186/s40580-021-00254-x](10.1186/s40580-021-00254-x).

26. Yu X., Wei D., Habib S., Liu H, Mahmud S., 2024. Efficient hydrogen evolution activity of NiMoP electrodeposited on stainless steel mesh, *Colloids Surf., A*, 696, 134278. DOI: 10.1016/j.colsurfa.2024.134278.